ACS APPLIED NANO MATERIALS

www.acsanm.org Article

Gold Nanoparticles Grown by Galvanic Replacement on Graphene-Coated Aluminum Panels as Large-Area Substrates for Surface-Enhanced Raman Scattering

Chia-Jung Chang, Chao-An Liu, Yu-Hsin Pu, Ting-Yu Yang, Hsiang-Ting Chiu, Chun-Hu Chen,* and Genin Gary Huang*

Cite This: *ACS Appl. Nano Mater.* 2020, 3, 5783−5793 Read Online

ACCESS | Metrics & More | Article Recommendations | Supporting Information

ABSTRACT: Galvanic replacement (GR) is a widely used method to obtain substrates with nanostructure morphologies. However, there are substantial challenges related to the uniformity of the deposited nanostructures, the preparation of large-area nanocomposites, and the alteration of the morphologies deposited on substrates. Graphene was introduced into the surface of the aluminum panels in this study prior to conducting the GR reaction to incorporate graphene advantages of extremely high electrical conductivity and electron mobility. The experimental results revealed that the morphological consistency and particle densities of gold nanoparticles deposited on panels with graphene were much higher than those deposited on panels without graphene. Moreover, gold nanoparticles were deposited on the surfaces with graphene prior to deposition on those without graphene. Ordered large-area gold/graphene/aluminum hybrid nanocomposites can be obtained with desired morphologies by altering the preparation conditions. Finally, the feasibility of using the as-prepared gold hybrid nanocomposites as surface-enhanced Raman scattering (SERS) substrates was examined. The results indicated that the Raman signal enhancement factors of the as prepared substrates were varied as the preparation condition changed due to the difference in the morphologies. Under the optimal condition, a high enhancement factor of approximately 3×10^8 with good reproducibility was found, which demonstrates the potential of utilizing the as-prepared gold hybrid nanocomposites in SERS and other sensing applications.

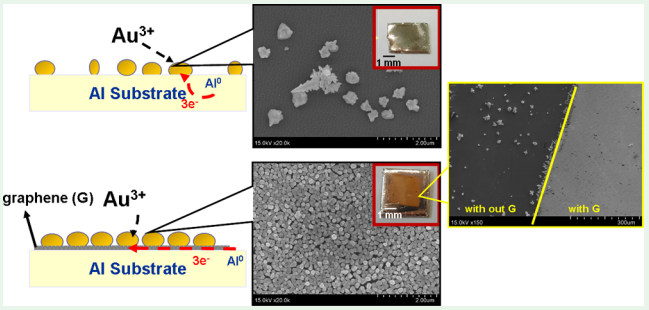

KEYWORDS: *galvanic replacement, graphene, large-area nanocomposite, SERS, surface-enhanced Raman scattering*

INTRODUCTION

In the past few decades, galvanic replacement (GR) has been widely used in the preparation of nanomaterials and has attracted increased research interests. Spontaneous oxidation−reduction reactions occur, and nanocomposites with different morphologies can be obtained due to the different reduction potentials between different metals. Although the relatively lower reproducibility of deposited nanostructures has limited their application, GR reaction-based nanocomposite fabrication has still been attracting substantial research attention because of its advantages of fast product preparation, cost effectiveness, and mass production potential. Different nanomaterial morphologies, such as nanocubes,[1] nanohexagonal particles,[2] nanodendrites,[3,4] nanoparticles,[5,6] nanorods,[7,8] nanobelts,[9] and others,[10−12] can be fabricated using GR reactions. Consequently, GR-based nanocomposites have been applied to various fields, such as catalysis,[7,13,14] biosensing,[15−17] surface-enhanced Raman scattering (SERS),[10,18−21] and electrochemical applications.[8,22]

SERS, one of the key applications of nanomaterials, has attracted considerable interests because it can provide higher sensitivity than conventional Raman spectroscopy, selective detection, water-free interference, and abundant chemical information. It is believed that the signal enhancement of Raman intensity can be attributed mostly to the electromagnetic enhancement (EM) while the contribution from the charge transfer mechanism (CT) is also significant. EM is related to the morphologies of the substrates, and CT is related to the molecule−substrate charge transfer at the Fermi levels.[23−25] SERS has been utilized in diverse research fields due to these advantages, such as forensic science,[26−29] biosensing,[30−33] medical applications,[32,34−36] environmental

Received: April 9, 2020
Accepted: June 2, 2020
Published: June 2, 2020

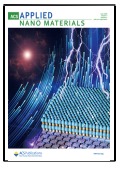

analysis,[37] and catalysis.[38,39] Although SERS has been studied extensively, it has several limitations related to the reproducibility of substrate morphologies, the stability of the substrates, and the restriction of substrates pertaining to substantial localized surface plasmon resonance (LSPR) behavior.

Attempts have been made to improve the uniformity of substrate morphology to overcome the aforementioned limitations pertaining to the SERS technique, such as thermal evaporation deposition,[40,41] evaporative self-assembly,[31,42,43] interfacial self-assembly,[44−47] and template-assisted fabrication.[48−52] The GR reaction has also been tried for fabricating reproducible nanocomposites.[19,21,50,53]

Owing to the excellent electron conductivity, high electron mobility, high loading ratio, and other fascinating properties, graphene has been used in the fabrication of nanocomposites.[54−60] Several studies further incorporated graphene with a GR reaction to fabricate hybrid nanocomposites.[3,13,58,59,61] The nanoparticle densities of the nanocomposites prepared using graphene are better than those without graphene. However, the aforementioned studies mostly focused on increasing the loadings of nanoparticles of the substrates. Though few studies tried to ameliorate the morphology inconsistency and the loading capacity by fabricating large-scale ordered nanocomposites,[54,59,60] multiple steps of transfer as well as deposition procedures were required, and the nanostructures on the nanocomposites are hardly tuned since the nanostructures were prepared before assembling on the substrates. Studies pertaining to the application of graphene for the preparation of large-area nanocomposites and the tuning of nanostructures deposited through a GR reaction have barely been reported. In this study, a simple and feasible method based on a GR reaction was proposed for preparing large-area gold hybrid nanocomposites. In the approach, a single layer of high-quality graphene is transferred onto the surface of electropolished aluminum panels before the GR reaction is conducted. The schematic of the method proposed in this study is illustrated in Scheme 1. As the panels were immersed

Scheme 1. Schematic Diagram of the Formation of Au Hybrid Nanocomposites[a]

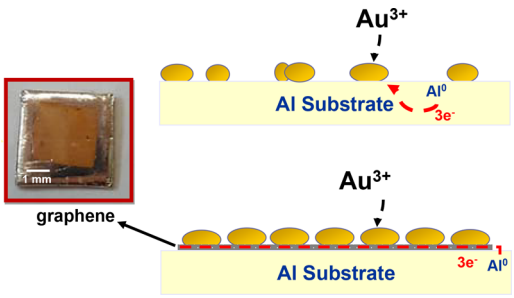

[a]With the high horizontal conductivity of graphene, the oxidation of Al without the protection of graphene takes place prior to that protected by graphene.

in the plating solution, a spontaneous oxidation of aluminum and reduction of Au^{3+} were driven by the difference in the reduction potentials between gold and aluminum. The high conductivity and electron mobility of graphene increased the electron transfer efficiency between Au^{3+} and Al substrates. Moreover, gold nanoparticles (AuNPs) were expected to be deposited on the positions with superior electron transit abilities, thus causing the morphologies of the deposited Au nanostructures to be more uniform. It is remarkable that the size and morphology of the deposited AuNPs can simply be tuned by varying the conditions of GR reactions. To the best of our knowledge, this study is the first attempt to fabricate large-area hybrid nanocomposites with ordered nanostructures by incorporating GR and graphene. The large-area ordered nanostructure of the hybrid nanocomposites enables the use of the as-prepared gold hybrid nanocomposites in a wide variety of applications.

EXPERIMENTAL SECTION

Materials. Aluminum foil (99.99%; thickness, 0.5 mm), hydrogen tetrachloroaurate, *p*-aminothiophenol (*p*ATP), ammonium persulfate, and sodium iodide were purchased from Alfa Aesar. Perchloric acid and poly(methyl methacrylate) (PMMA; MW, ~996 000) were obtained from Sigma-Aldrich. Sodium sulfate, sodium chloride, sodium bromide, and sodium hydroxide were obtained from Showa Chemical. Toluene was obtained from Avantor, and anhydrous ethanol was purchased from Echo Chemical, Taiwan. All the chemicals were of reagent grade and were used as received without further purification. Deionized Milli-Q water (Simplicity, Millipore) was used throughout the study.

Electropolishing of Aluminum Panels. Aluminum panels (AlPs) with thicknesses of 0.5 mm were used as the substrates in this study. The AlPs were electropolished using a DC power supply to remove the oxidation layer before further processing. In the electropolishing process, the AlPs with the desired dimensions were used as the anodes; a 1 × 1 cm^2 platinum plate was used as the cathode, and 25 mL of perchloric acid ethanol solution (20% v/v) was used as the electrolyte solution. The process was conducted by applying 25 V for 5 min in an ice bath. The electropolished AlPs were washed with ethanol and were directly subject to further treatments.[62]

Fabrication of Graphene and Graphene Hybrid AlPs. Single-layer graphene films were prepared on Cu foils through chemical vapor deposition (CVD).[63] In brief, Cu foils with the specified shapes and dimensions were placed in a quartz tube at 10^{-3} Torr. The CVD system was then heated up to 1000 °C with a hydrogen-gas flow of 10 sccm for 20 min to clean and anneal the Cu surface. Subsequently, the atmosphere of the foils was changed to a mixture of CH_4 (10 sccm) and H_2 (35 sccm), and the foils were maintained in this atmosphere for 40 min. Finally, the system was cooled to room temperature under argon gas flow (60 sccm). The graphene produced on the Cu foils was coated with a thin layer of PMMA by using spin coating. The Cu foils were then removed using ammonium persulfate solution. The obtained PMMA/graphene layers were transferred to the electropolished AlPs,[62,64] as described in the previous section. These layers were then dried for 10 min. Finally, the PMMA was dissolved using toluene to produce graphene hybrid aluminum panels (GAlPs) with a single graphene layer. GAlPs with different graphene layers can be produced by repeating the transfer procedure.

Gold Hybrid Nanocomposite Fabrication. The GR reaction was used in this study to deposit AuNPs on the AlPs and GAlPs by immersing AlPs and GAlPs (5 × 5 mm^2) into 3 mL of $HAuCl_4$ aqueous solutions at different concentrations. After a specified duration, the panels were removed and washed with deionized water and ethanol. To investigate the effects of anions, different anions with various concentrations were added to prepare the solutions with specific [Au^{3+}] to [anion] ratios. A cold field-emission scanning-electron microscope (FE-SEM; SU8010, Hitachi) equipped with an energy dispersive spectrometer (EDS; X-Stream, OXFORD INCA) was employed at accelerating voltages of 5.0, 10.0, and 15.0 kV to observe the morphologies of the fabricated gold hybrid nanocomposites.

SERS Measurements. The Raman signals of *p*ATP were acquired for the SERS experiments by using a Raman spectrometer system (*i*-Raman, B&W Tek, Inc.) with a 785 nm diode laser as the excitation source. A microsampling system (BAC151A, B&W Tek, Inc.)

https://dx.doi.org/10.1021/acsanm.0c00846
ACS Appl. Nano Mater. 2020, 3, 5783−5793

equipped with an objective lens with a numerical aperture of 0.25 (10× PlanC Objective, Olympus) was coupled with the Raman spectrometer to focus the excitation line and to collect the enhanced Raman scattering signal. The prepared hybrid nanocomposites with different morphologies were immersed in *p*ATP ethanol solution with a concentration of 1 mM for 1 h. The gold hybrid nanocomposites were rinsed with ethanol twice to remove the unadsorbed *p*ATP molecules before measurements were conducted. The laser power was 23.7 mW at the sample position; the exposure time of each SERS spectrum was 5 s with 10 accumulations, and all the measured Raman spectra had a resolution of 3 cm^{-1}. Sixteen different points on each nanocomposite were selected to measure the SERS spectra of *p*ATP to validate the stability and reproducibility of the substrates. An imaging spectrometer (iHR-320, HORIBA Jobin Yvon) equipped with a liquid-nitrogen-cooled charged-coupled device camera (Symphony, HORIBA Jobin Yvon) coupled with an Olympus BX41 microscope equipped with an Olympus PlanC N 40× objective lens (numerical aperture of 0.65) was used for measuring the Raman spectra of graphene. The 632.9 nm line of a He−Ne laser (25-LHP-925-245, Melles Griot) was used as the excitation source, and the laser power was 15 mW at the sample position.

RESULTS AND DISCUSSION

Characterization of Graphene on AlPs and the Fabricated Au Nanocomposites. Raman spectra of GAlPs with different layers of graphene were measured to confirm the successful transfer of graphene on AlPs (Figure 1). The figure

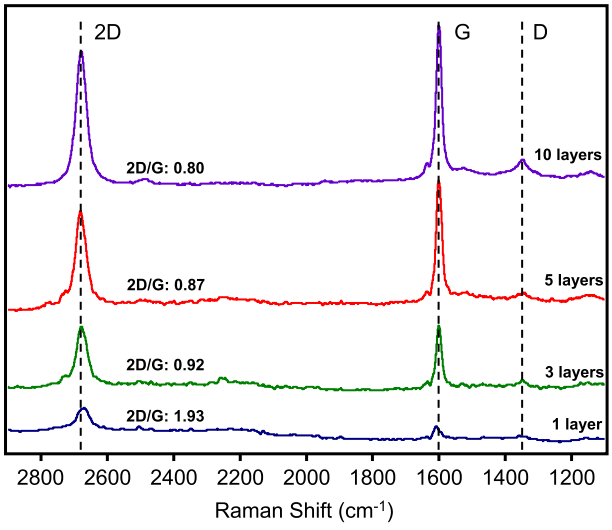

Figure 1. Conventional Raman spectra of GAlPs with different layers of graphene. From bottom to top: 1 layer, 3 layers, 5 layers, and 10 layers, respectively.

shows that the characteristic 2D band of a single layer of graphene was found at 2673 cm^{-1} and shifted to 2680 cm^{-1} as the number of graphene layers increased. For the characteristic G band, the observed wavelength was 1608 cm^{-1} and shifted to 1600 cm^{-1} as the number of graphene layers increased. A negligible D band observed at 1349 cm^{-1} showed the high quality of CVD graphene with a low defect level. The Raman spectra of a single layer of graphene to 10 layers of graphene revealed a typical increasing trend of 2D/G-band ratios from 1.93 to 0.80 and a slight peak shift of 2D bands, which is consistent with previous studies.[63,65,66] It is noted that the Raman signal of graphene is vanished in the Raman spectra of the prepared hybrid nanocomposites. It may be due to graphene being blocked by AuNPs so that the Raman signal of graphene can no longer be detected.

Graphene is expected to accelerate the electron transfer between Au^{3+} and GAlPs due to its extremely high electrical conductivity and electron mobility. Because AuNPs were deposited on the positions with superior electron transit abilities, the formed Au hybrid nanocomposites are expected to have more uniform morphologies, higher AuNPs densities, and higher charge transfer efficiencies. Figure 2a displays a

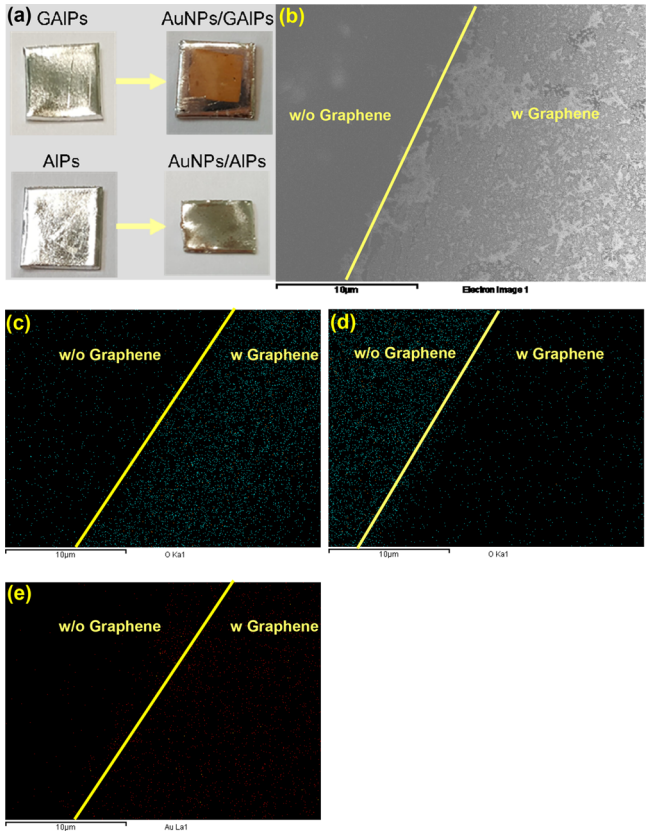

Figure 2. (a) Photograph of the GAlPs and AlPs before and after the deposition of AuNPs, respectively. (b) SEM image of the boundaries of AuNPs/GAlPs nanocomposites. EDS mapping analysis of oxygen element on the GAlPs before (c) and after (d) the GR reaction. (e) EDS mapping analysis of gold element on the GAlPs after the GR reaction.

photograph of the GAlPs and AlPs observed before and after the deposition of AuNPs, respectively. AuNPs were deposited on the GAlP substrate surfaces with graphene before AuNPs were deposited on those without graphene. However, AuNPs were deposited randomly on the surfaces of AlP substrates. Figure 2b depicts the SEM image of the boundaries of Au graphene hybrid nanocomposites to present the information at the microscopic level. The figure reveals that AuNPs deposited on the sides of the surfaces with graphene exhibited high density. Moreover, those AuNPs deposited on the sides without graphene appeared aggregated, and the amount of the deposited AuNPs was much smaller. It is assumed that graphene protected the aluminum atoms under graphene from oxidation since the vertical conductivity of graphene is rather poor. Aluminum atoms not covered by graphene were estimated to be oxidized prior to those covered by graphene, and the produced electrons were transferred to the graphene

https://dx.doi.org/10.1021/acsanm.0c00846
ACS Appl. Nano Mater. 2020, 3, 5783−5793

immediately due to the advantage of excellent horizontal conductivity of graphene (Scheme 1). Formation of an oxidation layer on bare aluminum is expected, which makes it no more capable of reducing AuNPs on the oxidation layer. Without the disturbance of oxidized aluminum atoms, the deposited AuNPs on GAlPs were able to pack as close as possible. EDS mapping analysis of oxygen was conducted on the GAlPs before and after deposition of AuNPs to further analyze the surface composition of the nanocomposites. Figure 2c shows the EDS mapping results of GAlPs before performing GR. It can be observed that the surface with graphene has a relatively higher signal of oxygen. However, after conducting the GR reaction, the relative signal of oxygen increased dramatically on bare aluminum sides as can be observed in Figure 2d, implying that aluminum sides without graphene oxidized before those with graphene and thus resulting in the observed morphologies. Figure 2e displays the EDS mapping of gold on GAlPs after the GR reaction, thus confirming that AuNPs were deposited on GAlPs. It is reported that gold nanoparticles can be reduced on graphene by the oxidation of graphene itself.[61] We have tried to replace aluminum panels with silicon wafers, and only very limited AuNPs were deposited on graphene/silicon panels where no AuNPs deposited on bare silicon panels. Further, the measured *p*ATP SERS intensities on AuNPs/GAlPs are ~10^2 times higher than those on AuNPs deposited on graphene/silicon panels (data not shown). Thus, the electrons required for depositing AuNPs are mostly provided by the oxidation of Al panels in this study as aforementioned.

Effect of Temperature and Duration of Displacement on the Preparation of Au Nanocomposites. One of the key factors that dominate the morphologies of the deposited AuNPs in the preparation of Au nanocomposites through the GR reaction is temperature, as it influences the deposition rate of AuNPs. Moreover, the displacement duration controls the sizes and morphologies of the deposited AuNPs. AlPs and GAlPs were immersed in 1 mM $HAuCl_4$ aqueous solutions at different temperatures and for different durations to study how temperature and displacement duration influence the morphologies of Au nanocomposites. Figure 3 displays the SEM images of the fabricated Au nanocomposites deposited with different displacement times at 0 and 60 °C. The deposition temperature and duration increased for the AuNPs deposited on AlPs. Moreover, the densities of the AuNPs deposited on AlPs increased significantly. However, poor uniformity of the AuNPs morphologies was observed on AlPs because the oxidation of Al occurred around the positions of AuNP deposition, which blocks the reduction of AuNPs on the oxidation layers. Meanwhile, without graphene, the initial nucleation of Au on AlPs is random, and the reduction of AuNPs was subsequently conducted on Au nuclei prior to the aluminum surface. At longer deposition times, dendritic morphologies of Au were observed on AlPs. Moreover, the aggregation of AuNPs was observed, especially at higher temperatures. The densities of AuNPs deposited on GAlPs are much greater than those of AuNPs deposited on AlPs. Moreover, the uniformity of the deposited AuNPs increased substantially. As detailed in the previous section, this substantial increase can be attributed to the extremely high electron transfer efficiency of graphene, thus resulting in the even formation of numerous Au nuclei on the graphene sheet. As the deposition temperature or duration increased, the high densities of the AuNPs on GAlPs remained almost unchanged;

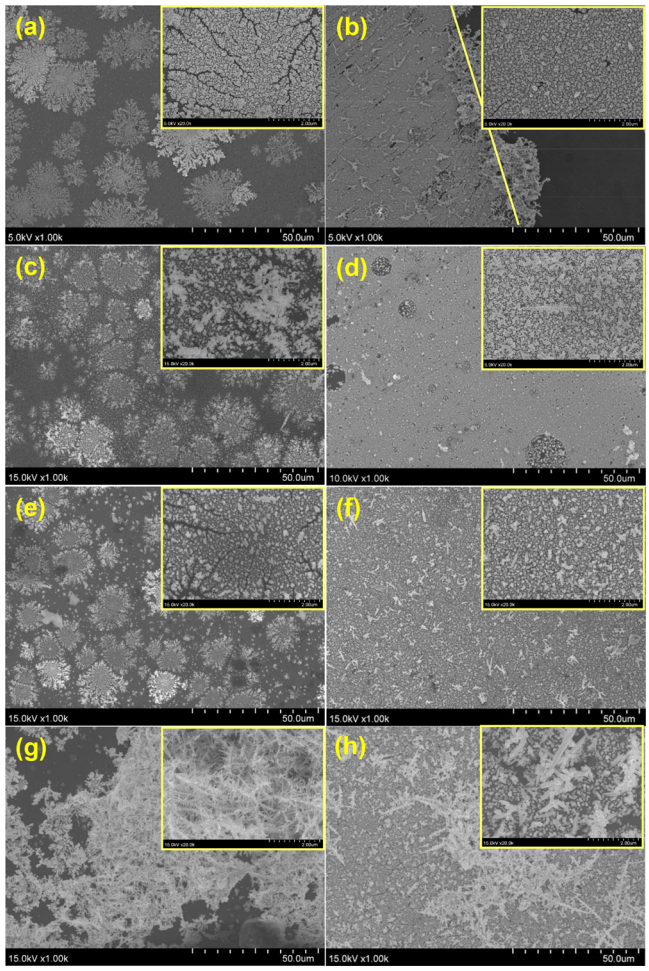

Figure 3. SEM images of fabricated Au hybrid nanocomposites (a, c, e, g, AuNPs on AlPs; b, d, f, h, AuNPs on GAlPs) with different displacement times (a, b, e, f, 60 min; c, d, g, h, 120 min) where the temperatures are 0 °C (a–d) and 60 °C (e–h), respectively.

however, the sizes of the AuNPs increased, and dendritic morphologies were noted. This finding demonstrates that the temperature and displacement duration influence the sizes and consistencies of AuNPs deposited on AlPs. However, the consistencies of AuNPs on GAlPs were almost unaffected because the initial nucleation of Au on GAlPs occupies almost all the hot sites with higher electron transferability of the graphene sheet (more SEM images of AuNPs on AlPs and GAlPs prepared at different temperatures are plotted as Figure S1 in the Supporting Information). The fabricated Au nanocomposites were immersed in 1 mM *p*ATP, and their SERS spectra were recorded to examine the adequacy of using the prepared Au nanocomposites as SERS active substrates and to further correlate the AuNP morphologies with SERS signal intensities. Figure 4 presents the typical *p*ATP SERS spectra detected by the Au nanocomposites fabricated in this study. The measured peak positions and their band assignments are tabulated in Table S1. It is found that the peak located at 1087 cm^{-1}, which was assigned as the C–S stretching of *p*ATP, was shifted to 1078 cm^{-1} after adsorbing on the surface of nanocomposites. Meanwhile, the S–H stretching vibration located at 2551 cm^{-1} was absent in the obtained SERS spectra. These findings suggest the chemisorption of *p*ATP on the nanocomposites. The spectra and table reveal that the peak

https://dx.doi.org/10.1021/acsanm.0c00846
ACS Appl. Nano Mater. 2020, 3, 5783–5793

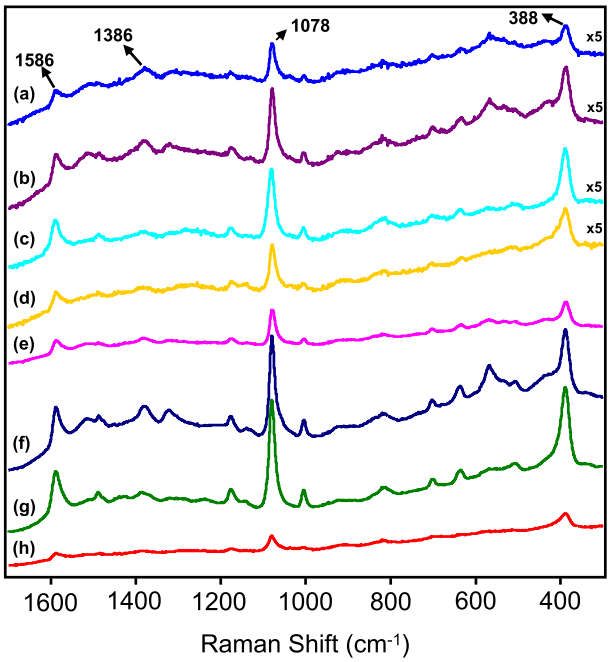

Figure 4. SERS spectra of *p*ATP obtained by different AuNPs hybrid nanocomposites (a–d, AuNPs/AlPs; e–h, AuNPs/GAlPs) prepared with different displacement times (a, c, e, g, 60 min; b, d, f, h, 120 min) and temperatures (a, b, e, f, 0 °C; c, d, g, h, 60 °C) where $[Au^{3+}]$ are all 1 mM.

positions of *p*ATP obtained using Au nanocomposites fabricated in this study exhibit a slight shift compared with those observed in previous studies, which is due to the different morphologies and the structures of the substrates used,[25,60,67,68] although b_2 vibrational modes of phenyl rings, which imply the presence of a charge transfer mechanism, were observed.[60,67,69,70] The relative intensities of a_1 modes are much higher than b_2 modes, thus suggesting that the Raman signal enhancement of the as-prepared hybrid nanocomposites is mainly contributed by the electromagnetic enhancement (EM) mechanism. Besides, several studies have reported that *p*ATP molecules adsorbed on noble nanoparticles can be chemically transformed to 4,4′-dimercaptoazobenzene (DMAB), and the observed b_2 vibrational modes of the aromatic ring is contributed by DMAB.[70−72] Although b_2 modes of the aromatic rings were also observed in the SERS spectra measured with AuNPs/GAlPs nanocomposites, the relative intensity is weak and did not vary with irradiated time. Besides, a longer wavelength of NIR laser (785 nm) was used as an excitation source, and the power is only around 13 W/mm^2. Thus, the photoinduced transformation of *p*ATP to DMAB did not happen in this study. Figure 5a presents a peak of the SERS intensity at 1078 cm^{-1} using AuNPs deposited on AlPs as substrates versus deposition time at different temperatures. The figure shows that the SERS intensities of *p*ATP increased as the deposition duration increased and attained a maximum value at 60 min under temperatures of 0, 40, and 60 °C. Here, the SERS intensities of *p*ATP achieved their maximum values at 120 min under room temperature (RT). Moreover, the enhancement factors of Au nanocomposites fabricated at RT are generally higher than those of Au nanocomposites fabricated at other temperatures. To show the enhancement factor of the AuNPs deposited on GAlPs, Figure 5b plots the SERS intensities of *p*ATP versus

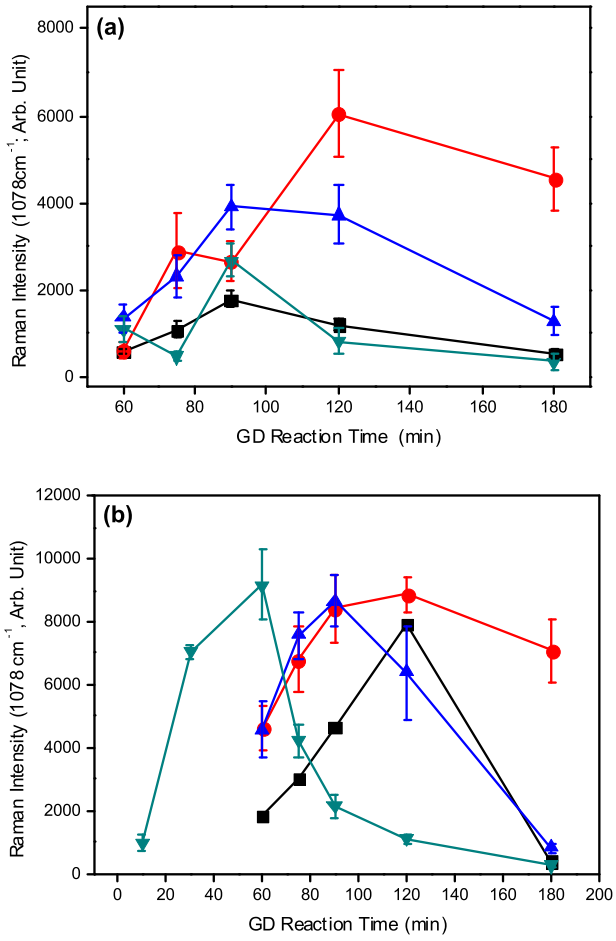

Figure 5. SERS intensities of *p*ATP measured by (a) AuNPs/AlPs and (b) AuNPs/GAlPs nanocomposites versus the deposition time under different temperatures (■, 0 °C; ●, RT; ▲, 40 °C; ▼, 60 °C).

deposition time at different temperatures; a slight deviation in behaviors was observed. The SERS intensities of *p*ATP increased as the deposition duration increased and attained a maximum intensity. Moreover, the duration of attaining the maximum enhancement factors is dependent on temperature; for a lower temperature, a longer deposition time is required, and at a higher temperature, the maximum SERS intensity was achieved earlier. The maximum SERS intensity for AuNPs deposited on GAlPs were close to each other, thus suggesting that the temperature and duration of deposition vary the sizes of the deposited AuNPs but do not influence the densities of AuNPs. Moreover, the SERS intensities of *p*ATP obtained using AuNPs deposited on GAlPs are further enhanced compared with those of *p*ATP obtained using AuNP deposition on AlPs. Other than the enhancement factor, the relative standard deviation (RSD) of the obtained signal is also an important factor to evaluate the adequacy of the prepared substrates to be used as SERS active substrates. For AuNPs/AlPs nanocomposites, the RSD of the maximum SERS signal are varied from 17.0% to 22.1% depending on the temperatures of the GR reaction. In contrast, the RSD of the maximum SERS signal obtained with AuNPs/GAlPs nanocomposites apparently decreased to 6.1−12.1% with different displacement temperatures. These findings are consistent with the morphologies observed in SEM images, which implies that

https://dx.doi.org/10.1021/acsanm.0c00846
ACS Appl. Nano Mater. 2020, 3, 5783−5793

GAlPs are better substrates than AlPs for the preparation of Au hybrid nanocomposites by the GR reaction.

Effect of Au^{3+} Concentration Used in Galvanic Displacement. In addition to the temperature, the concentration of Au^{3+} used in the GR reaction controls the morphologies of the deposited AuNPs because the concentration of the Au^{3+} influences the AuNPs deposition rate. AlPs and GAlPs were immersed in different concentrations of $HAuCl_4$ aqueous solutions at 0 °C to examine how the concentration of Au^{3+} used in GR deposition influences the morphologies of Au nanocomposites. Figure S2 displays the SEM images of the Au nanocomposites fabricated using different Au^{3+} concentrations. Similar to the effects of temperature, AuNPs deposited on AlPs and GAlPs had different behaviors. Under low Au^{3+} concentrations, AuNPs were found to deposit on formed Au nuclei prior to deposition on Al surfaces so that the densities of the AuNPs on AlPs are rather low, and aggregated morphologies are found. As the concentration of Au^{3+} increased, the densities of the AuNPs increased gradually on AlPs. However, the uniformity of the AuNPs on AlPs was still poor. For the AuNPs deposited on GAlPs, the AuNPs were evenly spread over the GAlPs with maximized densities under all Au^{3+} concentrations. Moreover, the concentration of Au^{3+} mostly influenced the sizes of the deposited AuNPs. Three-dimensional dendritic Au nanomorphologies were observed when the concentration of Au^{3+} was 2 mM, as demonstrated in the deposition temperature section.

Figure 6a,b plots the SERS intensities of *p*ATP versus the deposition time under different Au^{3+} concentrations using AuNPs/AlPs and AuNPs/GAlPs as substrates to further study the Raman signal enhancement capability of the fabricated Au nanocomposites. Figure 6a shows that when the Au^{3+} concentration is 0.05 mM, the fabricated Au nanocomposites reveal almost no Raman signal enhancement unless the deposition time is 240 min. When the Au^{3+} concentration was increased to 0.1 mM, the SERS intensities of *p*ATP increased with deposition duration and attained a maximum value at 120 min. The duration required to achieve the signal enhancement maxima was reduced to 90 min when the Au^{3+} concentrations of 0.5 and 1 mM were used. The SERS signal was reduced gradually as the duration of deposition increased after the signal maxima was achieved, thus suggesting that the AuNPs were too large to obtain the optimal SERS effect. The Au^{3+} concentration of 2 mM provides the longest deposition time to attain the signal maxima at 180 min, and the SERS signal was fixed, even when the deposition time was extended to 240 min. According to the results detailed in the figure, Au^{3+} concentrations of 0.5 or 1 mM are suggested to obtain AuNPs/AlPs substrates with the highest SERS signal enhancement factors.

Figure 6b reveals that, for the enhancement factor of the AuNPs/GAlPs substrates, the SERS intensities of *p*ATP increased with the deposition time and attained a maximum intensity. This increase was followed by the reduction of the SERS signal until AuNP deposition is complete. Moreover, the durations of attaining the maximum enhancement factors and the signal maxima are both dependent on Au^{3+} concentration. Here, lower Au^{3+} concentrations achieved signal maxima faster but with relatively small enhancement factors. However, higher Au^{3+} concentrations require longer deposition times to attain signal maxima, and the enhancement factors obtained were higher than those of lower Au^{3+} concentrations. Similarly, the

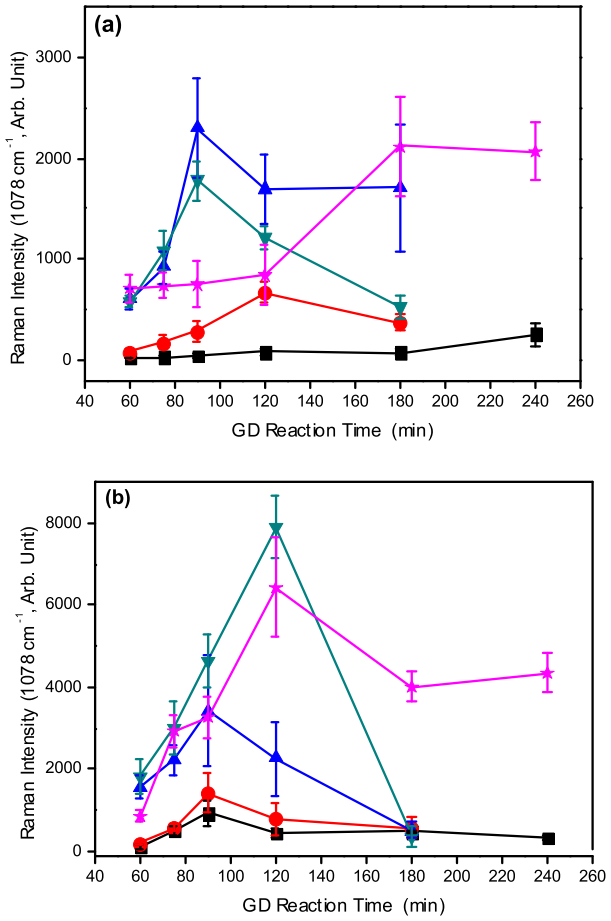

Figure 6. SERS intensities of *p*ATP measured by (a) AuNPs/AlPs and (b) AuNPs/GAlPs nanocomposites versus the deposition time under different [Au^{3+}] (■, 0.05 mM; ●, 0.1 mM; ▲, 0.5 mM; ▼, 1 mM; ★, 2 mM) where the temperature is 0 °C, and the GR reaction times are all 120 min.

SERS intensities of *p*ATP obtained using AuNPs deposited on GAlPs were more enhanced than those of *p*ATP obtained using AuNPs/AlPs. The SERS signal was further enhanced by approximately 20 times under a Au^{3+} concentration of 0.05 mM when the deposition time was 90 min, whereas the SERS signal was further enhanced by a factor of 6.50 when the deposition time was 90 min and the Au^{3+} concentration was 1 mM. To examine the quantitative performance of the as-prepared AuNPs/GAlPs hybrid nanocomposites, Figure S3 plotted the concentration-dependent SERS intensities of *p*ATP, and the relative intensities were fitted by a Gaussian curve fit. One can see the remarkable increase in the SERS intensities over a large range of concentrations, which demonstrates the ability of the AuNPs/GAlPs hybrid nanocomposites in quantitative measurements. To further examine the performance of the AuNPs/GAlPs nanocomposites, the enhancement factor of the prepared gold hybrid nanocomposites was also evaluated. Figure S4 plotted the conventional Raman spectra and the obtained SERS spectrum of *p*ATP. By correlating the relative numbers of deposited molecules and the relative Raman signal, an enhancement factor of 3×10^8 can be calculated.

Effect of Anions and pH on Au Nanocomposites. Au nanocomposites with different morphologies can be obtained by adjusting the GR reaction temperature, Au^{3+} concentration,

https://dx.doi.org/10.1021/acsanm.0c00846
ACS Appl. Nano Mater. 2020, 3, 5783−5793

and deposition duration. Moreover, the deposited AuNPs had extremely high particle density and morphology uniformity when GAlPs were used as substrates. Different anions were added to the plating solutions to further control the morphologies of the deposited AuNPs. The reduction of gold is expected to be gentle due to the formation of gold(III) complexes. Moreover, the negatively charged gold complex ions are estimated to deposit on the substrates separately to reduce repulsion. Different anions, including sulfate, chloride, bromide, and iodide, with different logarithm stability constants with gold(III) of 6, 26, 32, and 47, respectively, were added in the plating solution to confirm these expectations.[73] Figure S5 displays the SEM images of Au nanocomposites in the absence and presence of different anions. For the AuNPs deposited on AlPs, the addition of anions in the Au^{3+} solutions did not increase the densities or the morphological consistency of the deposited AuNPs. By contrast, the presence of anions significantly influenced the morphologies of AuNPs deposited on GAlPs. Due to the repulsion between the gold complex ions, the AuNPs with anions were much more likely to be spherical in shape than those without anions. Moreover, the sizes and densities of the deposited AuNPs seemed to be related to the formation constants between Au^{3+} and anions used. For example, the largest AuNP sizes and the lowest AuNP densities are obtained in the presence of iodide, which has the highest formation constants with Au^{3+} among the examined anions. Figure S6 shows the SEM images of AuNPs on AlPs and GAlPs with different iodide concentrations. As the iodide concentration increased, the sizes of AuNPs increased, and the densities of AuNPs deposited on GAlPs decreased gradually where the morphologies of AuNPs deposited on AlPs did not show the dependency of iodide concentrations. The results reveal that more spherical AuNPs can be obtained by adding anions as additives. Moreover, the sizes, particle densities, and shapes of Au nanostructures deposited on GAlPs can be tuned by selecting different anions with different concentrations.

Compared with the anions examined previously, hydroxide can also form stable complex ions with Au^{3+} ($\log K = 55$). Hence, the pH of the gold solutions can also influence the morphologies of Au nanocomposites prepared in this study. The pH of the 1 mM Au^{3+} solution was adjusted from 2.5 to 10, and the GR reaction was conducted at RT for 90 min to study how the morphologies are influenced by pH. Figure 7 displays the SEM images of AuNPs deposited on AlPs and GAlPs under different pH values. Similar to the effects of other anions, the sizes of AuNPs deposited on AlPs and GAlPs increased as the pH increased because OH^- concentrations increase under higher pH values. The particle densities of AuNPs on GAlPs are also higher than those of AuNPs on AlPs. These observations indicate that the sizes and particle densities of AuNPs on GAlPs can be controlled by selecting suitable pH conditions. To further correlate the gold hybrid nanocomposites prepared under different pH values and their SERS enhancement capabilities, Figure S7 is presented, which plots the SERS intensities of *p*ATP obtained with gold hybrid nanocomposites prepared under different pH values. The correlation of Figure S7 and Figure 7 reveals that the sizes of the deposited AuNPs increased with an increase in pH, resulting in a significant decrease in enhancement factor because the sizes of the deposited AuNPs were too large to remain in an intense LSPR field.

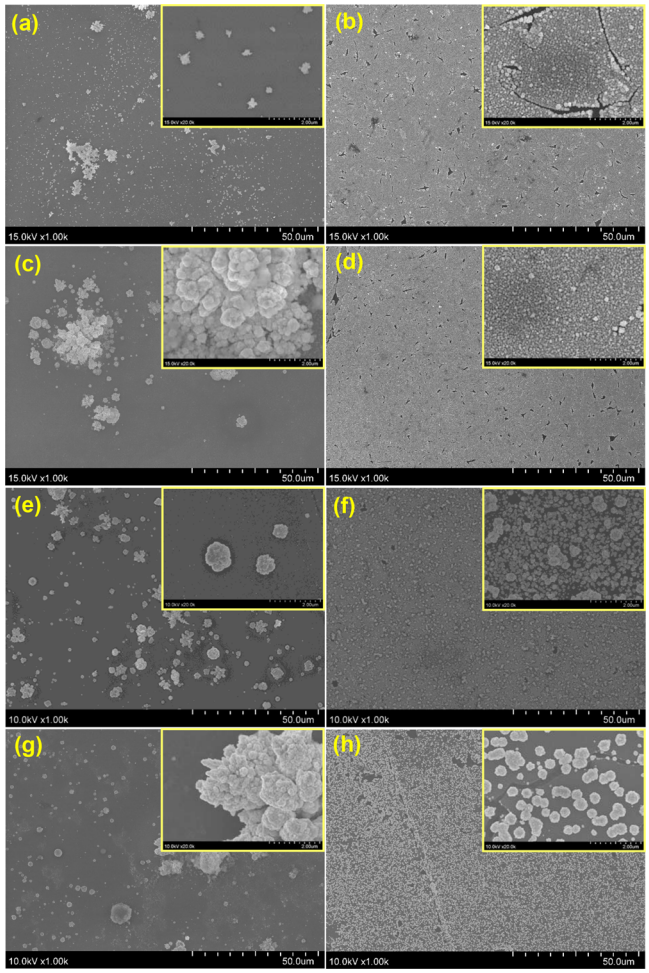

Figure 7. SEM images of fabricated Au hybrid nanocomposites (a, c, e, g, AuNPs/AlPs; b, d, f, h, AuNPs/GAlPs) under different pH values (a, b, pH = 2.5; c, d, pH = 4.0; e, f, pH = 8.0; g, h, pH = 10.0) where $[Au^{3+}]$ is 1 mM, deposition time is 90 min, and the temperatures are all RT.

Effect of Graphene Thickness in Preparing Au Nanocomposites. The electronic band structure of graphene along the direction parallel to the *c*-axis exhibits certain gaps, although graphene is widely known as a zero band gap material.[63] The stacking of graphene sheets results in discrete energy levels that are normal to the surface of graphene, which may influence the electron transferring efficiencies from the substrates to the top layer of graphene. On the basis of our assumptions, the function of graphene in GR is to protect AlPs by transferring the electrons produced on the sides without graphene to graphene with extremely high efficiency. Electrons are expected to transfer to K points of graphene before transferring to other places during the GR reaction because of the single joint point of valence and conduction bands at the K point. The electron motilities at the K point are expected to be higher than those at other points. Thus, the LSPR effect of AuNPs deposited on GAlPs is also expected to be more intense than the effect of those deposited on AlPs. This causes a difference in Raman signal enhancement capabilities. Therefore, the stacking of multiple layers of graphene may influence the morphologies of the deposited AuNPs and the enhancement factors when the prepared hybrid nanocomposites are used as SERS substrates. To study the influence of graphene

https://dx.doi.org/10.1021/acsanm.0c00846
ACS Appl. Nano Mater. 2020, 3, 5783−5793

thickness in the preparation of AuNP hybrid nanocomposites, AuNPs/GAlPs nanocomposites with different layers of graphene were prepared using a GR with conditions of 1 mM Au^{3+} at RT with a deposition time of 90 min. Figure 8

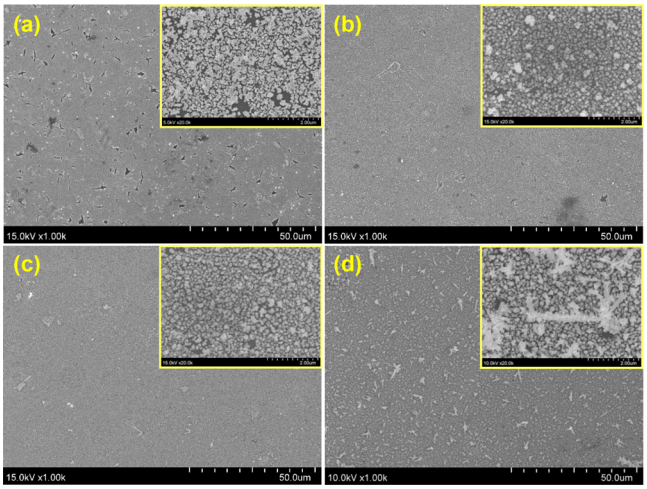

Figure 8. SEM images of Au hybrid nanocomposites in the presence of different layers of graphene (a, 1 layer; b, 3 layers; c, 5 layers; d, 10 layers) where $[Au^{3+}]$ is 1 mM, deposition time is 90 min, and the temperatures are all RT.

presents the SEM images of Au hybrid nanocomposites with different layers of graphene. The images reveal that the morphologies of the deposited gold nanomaterials are more likely to be spherical, and the gold nanostructures had fewer defects when three and five layers of stacked graphene are used, with more uniform morphologies obtained. When 10 layers of graphene were stacked, the sizes of the deposited AuNPs increased significantly (inset of Figure 8d), and dendritic morphologies were observed. Figure S8 displays the SERS intensities of *p*ATP using AuNPs deposited on GAlPs as substrates that are stacked with different layers of graphene. The figure reveals that the SERS signal enhancements are similar when one, three, and five layers of graphene are stacked, which reveals high agreement with the SEM images because the AuNP particle sizes with one, three, and five layers of graphene are similar. As the number of stacked graphene layers increased to 10, the Raman signal enhancement reduced drastically. The rapid decrease in Raman signal enhancement can be attributed to the fact that an extremely large number of stacked graphene layers was disadvantageous because the electron transition efficiencies between different layers of graphene were not as high as those within the same layer. This phenomenon influences the nucleation of Au in the first stage and leads to the formation of large Au nanoaggregates to produce a high electromagnetic enhancement.[23,74−76]

CONCLUSION

A GR reaction was used in this study for the preparation of gold hybrid nanocomposites. To further increase the morphologic reproducibility and densities of the deposited nanostructures, graphene was incorporated in the surface of the aluminum substrates before replacement to obtain the advantages of extremely high electrical conductivity and electron mobility of graphene. The experimental results revealed that the morphology consistency and particle densities of AuNPs deposited on GAlPs were much higher than those deposited on AlPs. Moreover, the AuNPs were deposited on the surfaces with graphene before depositing on surfaces without graphene because the surfaces without graphene oxidized, and electrons were transferred to the graphene immediately. This process results in an even formation of a large number of Au nuclei on graphene sheets.

Moreover, the morphologies of gold hybrid nanocomposites were influenced by the parameters of the preparation process of hybrid nanocomposites, such as $[Au^{3+}]$ concentration, displacement time, reaction temperature, pH value, number of graphene stacked layers, and the addition of other anions. Gold hybrid nanocomposites with desired morphologies can be obtained by optimizing the preparation conditions. To further examine the applicability of the nanocomposites, the as-prepared gold hybrid nanocomposites were used as SERS substrates, and a high enhancement factor of approximately 3×10^8 with good reproducibility was observed. These results reveal the potential of utilizing Au hybrid nanocomposites in SERS applications. The use of these nanocomposites in other applications, such as catalysis and biosensors, is under investigation.

ASSOCIATED CONTENT

Supporting Information

The Supporting Information is available free of charge at https://pubs.acs.org/doi/10.1021/acsanm.0c00846.

Band assignments of the obtained *p*ATP SERS spectra, more SEM images of AuNPs deposited AlPs and GAlPs with different preparation conditions, and the SERS spectra for estimating the enhancement factor (PDF)

AUTHOR INFORMATION

Corresponding Authors

Chun-Hu Chen − *Department of Chemistry, National Sun Yat-sen University, Kaohsiung 804, Taiwan;* orcid.org/0000-0002-3512-6880; Email: chunhu.chen@mail.nsysu.edu.tw

Genin Gary Huang − *Department of Medicinal and Applied Chemistry, Kaohsiung Medical University, Kaohsiung 807, Taiwan; Department of Medical Research, Kaohsiung Medical University Hospital, Kaohsiung 807, Taiwan; Department of Chemistry, National Sun Yat-sen University, Kaohsiung 804, Taiwan;* orcid.org/0000-0003-2241-1954; Email: genin@kmu.edu.tw

Authors

Chia-Jung Chang − *Department of Medicinal and Applied Chemistry, Kaohsiung Medical University, Kaohsiung 807, Taiwan*

Chao-An Liu − *Department of Medicinal and Applied Chemistry, Kaohsiung Medical University, Kaohsiung 807, Taiwan*

Yu-Hsin Pu − *Department of Medicinal and Applied Chemistry, Kaohsiung Medical University, Kaohsiung 807, Taiwan*

Ting-Yu Yang − *Department of Medicinal and Applied Chemistry, Kaohsiung Medical University, Kaohsiung 807, Taiwan*

Hsiang-Ting Chiu − *Department of Medicinal and Applied Chemistry, Kaohsiung Medical University, Kaohsiung 807, Taiwan*

Complete contact information is available at: https://pubs.acs.org/10.1021/acsanm.0c00846

https://dx.doi.org/10.1021/acsanm.0c00846
ACS Appl. Nano Mater. 2020, 3, 5783−5793

Notes

The authors declare no competing financial interest.

■ ACKNOWLEDGMENTS

We acknowledge the financial support from the Taiwan Ministry of Science and Technology under grant MOST107-2113-M-037-013 and NSYSU-KMU Joint Research Project, NSYSUKMU103-P015. This work is also supported by a grant from the Kaohsiung Medical University Research Foundation (KMU-M109025).

■ REFERENCES

(1) Polavarapu, L.; Liz-Marzán, L. M. Growth and Galvanic Replacement of Silver Nanocubes in Organic Media. *Nanoscale* **2013**, *5*, 4355−4361.
(2) Yamamoto, Y. S.; Fujime, Y.; Takahashi, N.; Nakanishi, S.; Itoh, T. Formation Mechanism of Plasmonic Silver Nanohexagonal Particles Made by Galvanic Displacement Reaction. *RSC Adv.* **2016**, *6*, 31454−31461.
(3) Fu, L.; Zhu, D.; Yu, A. Galvanic Replacement Synthesis of Silver Dendrites-Reduced Graphene Oxide Composites and Their Surface-Enhanced Raman Scattering Characteristics. *Spectrochim. Acta, Part A* **2015**, *149*, 396−401.
(4) Gutés, A.; Carraro, C.; Maboudian, R. Silver Dendrites from Galvanic Displacement on Commercial Aluminum Foil As an Effective SERS Substrate. *J. Am. Chem. Soc.* **2010**, *132*, 1476−1477.
(5) Chang, R.-L. J.; Yang, J. Surface-Controlled Electroless Deposition Method in the Preparation of Stacked Silver Nanoparticles on Germanium for Surface-Enhanced Infrared Absorption Measurements. *Appl. Spectrosc.* **2010**, *64*, 211−218.
(6) Porter, L. A.; Choi, H. C.; Ribbe, A. E.; Buriak, J. M. Controlled Electroless Deposition of Noble Metal Nanoparticle Films on Germanium Surfaces. *Nano Lett.* **2002**, *2*, 1067−1071.
(7) Nafria, R.; Luo, Z.; Ibáñez, M.; Martí-Sànchez, S.; Yu, X.; de la Mata, M.; Llorca, J.; Arbiol, J.; Kovalenko, M. V.; Grabulosa, A.; Muller, G.; Cabot, A. Growth of Au−Pd2Sn Nanorods via Galvanic Replacement and Their Catalytic Performance on Hydrogenation and Sonogashira Coupling Reactions. *Langmuir* **2018**, *34*, 10634−10643.
(8) Jeena, S.; Gnanaprakasam, P.; Selvaraju, T. Unusual Attempt to Direct the Growth of Bimetallic Ag@Pt Nanorods on Electrochemically Reduced Graphene Oxide Nanosheets by Electroless Exchange of Cu by Pt for an Efficient Alcohol Oxidation. *J. Nanopart. Res.* **2017**, *19*, 1−13.
(9) Liu, R.; Sen, A. Unified Synthetic Approach to Silver Nanostructures by Galvanic Displacement Reaction on Copper: From Nanobelts to Nanoshells. *Chem. Mater.* **2012**, *24*, 48−54.
(10) Pradhan, M.; Chowdhury, J.; Sarkar, S.; Sinha, A. K.; Pal, T. Hierarchical Gold Flower with Sharp Tips from Controlled Galvanic Replacement Reaction for High Surface Enhanced Raman Scattering Activity. *J. Phys. Chem. C* **2012**, *116*, 24301−24313.
(11) Ortiz, N.; Skrabalak, S. E. Controlling the Growth Kinetics of Nanocrystals via Galvanic Replacement: Synthesis of Au Tetrapods and Star-Shaped Decahedra. *Cryst. Growth Des.* **2011**, *11*, 3545−3550.
(12) Polavarapu, L.; Zanaga, D.; Altantzis, T.; Rodal-Cedeira, S.; Pastoriza-Santos, I.; Pérez-Juste, J.; Bals, S.; Liz-Marzán, L. M. Galvanic Replacement Coupled to Seeded Growth as a Route for Shape-Controlled Synthesis of Plasmonic Nanorattles. *J. Am. Chem. Soc.* **2016**, *138*, 11453−11456.
(13) Chen, J.; Lu, Z.-H.; Huang, W.; Kang, Z.; Chen, X. Galvanic Replacement Synthesis of NiPt/Graphene as Highly Efficient Catalysts for Hydrogen Release from Hydrazine and Hydrazine Borane. *J. Alloys Compd.* **2017**, *695*, 3036−3043.
(14) Cao, M.; Zhou, L.; Xu, X.; Cheng, S.; Yao, J.-L.; Fan, L.-J. Galvanic Replacement Approach for Bifunctional Polyacrylonitrile/Ag-M (M = Au or Pd) Nanofibers as SERS-Active Substrates for Monitoring Catalytic Reactions. *J. Mater. Chem. A* **2013**, *1*, 8942−8949.
(15) Gao, C.; Lu, Z.; Liu, Y.; Zhang, Q.; Chi, M.; Cheng, Q.; Yin, Y. Highly Stable Silver Nanoplates for Surface Plasmon Resonance Biosensing. *Angew. Chem., Int. Ed.* **2012**, *51*, 5629−5633.
(16) Zhang, Y.; Chen, M.; Cai, Z.; Zhang, M.; Liu, P.; Cheng, F. The Facile Synthesis of Branch-Trunk Ag Hierarchical Nanostructures and Their Applications for High-Performance H_2O_2 Electrochemical Sensors. *Sensors* **2017**, *17*, 2896.
(17) Loiseau, A.; Asila, V.; Boitel-Aullen, G.; Lam, M.; Salmain, M.; Boujday, S. Silver-Based Plasmonic Nanoparticles for and Their Use in Biosensing. *Biosensors* **2019**, *9*, 78.
(18) Wang, C.-H.; Sun, D.-C.; Xia, X.-H. One-Step Formation of Nanostructured Gold Layers via a Galvanic Exchange Reaction for Surface Enhancement Raman Scattering. *Nanotechnology* **2006**, *17*, 651.
(19) Li, Z.; Sun, K.; Du, Z.; Chen, B.; He, X. Galvanic-Cell-Reaction-Driven Deposition of Large-Area Au Nanourchin Arrays for Surface-Enhanced Raman Scattering. *Nanomaterials* **2018**, *8*, 265.
(20) Netzer, N. L.; Tanaka, Z.; Chen, B.; Jiang, C. Tailoring the SERS Enhancement Mechanisms of Silver Nanowire Langmuir−Blodgett Films via Galvanic Replacement Reaction. *J. Phys. Chem. C* **2013**, *117*, 16187−16194.
(21) Li, Z.; Meng, G.; Huang, Q.; Zhu, C.; Zhang, Z.; Li, X. Galvanic-Cell-Induced Growth of Ag Nanosheet-Assembled Structures as Sensitive and Reproducible SERS Substrates. *Chem. - Eur. J.* **2012**, *18*, 14948−14953.
(22) Xu, C.; Liu, Y.; Wang, J.; Geng, H.; Qiu, H. Fabrication of Nanoporous Cu−Pt(Pd) Core/Shell Structure by Galvanic Replacement and Its Application in Electrocatalysis. *ACS Appl. Mater. Interfaces* **2011**, *3*, 4626−4632.
(23) Ding, S.-Y.; You, E.-M.; Tian, Z.-Q.; Moskovits, M. Electromagnetic Theories of Surface-Enhanced Raman Spectroscopy. *Chem. Soc. Rev.* **2017**, *46*, 4042−4076.
(24) Lombardi, J. R.; Birke, R. L. A Unified View of Surface-Enhanced Raman Scattering. *Acc. Chem. Res.* **2009**, *42*, 734−742.
(25) Osawa, M.; Matsuda, N.; Yoshii, K.; Uchida, I. Charge Transfer Resonance Raman Process in Surface-Enhanced Raman Scattering from p-Aminothiophenol Adsorbed on Silver: Herzberg-Teller Contribution. *J. Phys. Chem.* **1994**, *98*, 12702−12707.
(26) Haddad, A.; Comanescu, M. A.; Green, O.; Kubic, T. A.; Lombardi, J. R. Detection and Quantitation of Trace Fentanyl in Heroin by Surface-Enhanced Raman Spectroscopy. *Anal. Chem.* **2018**, *90*, 12678−12685.
(27) Fedick, P. W.; Bills, B. J.; Manicke, N. E.; Cooks, R. G. Forensic Sampling and Analysis from a Single Substrate: Surface-Enhanced Raman Spectroscopy Followed by Paper Spray Mass Spectrometry. *Anal. Chem.* **2017**, *89*, 10973−10979.
(28) Rana, V.; Cañamares, M. V.; Kubic, T.; Leona, M.; Lombardi, J. R. Surface-Enhanced Raman Spectroscopy for Trace Identification of Controlled Substances: Morphine, Codeine, and Hydrocodone. *J. Forensic Sci.* **2011**, *56*, 200−207.
(29) Brettell, T. A.; Butler, J. M.; Saferstein, R. Forensic Science. *Anal. Chem.* **2005**, *77*, 3839−3860.
(30) Li, Y.; Gao, T.; Xu, G.; Xiang, X.; Zhao, B.; Han, X. X.; Guo, X. Direct Approach toward Label-Free DNA Detection by Surface-Enhanced Raman Spectroscopy: Discrimination of a Single-Base Mutation in 50 Base-Paired Double Helixes. *Anal. Chem.* **2019**, *91*, 7980−7984.
(31) Bi, L.; Wang, Y.; Yang, Y.; Li, Y.; Mo, S.; Zheng, Q.; Chen, L. Highly Sensitive and Reproducible SERS Sensor for Biological pH Detection Based on a Uniform Gold Nanorod Array Platform. *ACS Appl. Mater. Interfaces* **2018**, *10*, 15381−15387.
(32) Liang, L.; Qu, H.; Zhang, B.; Zhang, J.; Deng, R.; Shen, Y.; Xu, S.; Liang, C.; Xu, W. Tracing Sialoglycans on Cell Membrane via Surface-Enhanced Raman Scattering Spectroscopy with a Phenylboronic Acid-Based Nanosensor in Molecular Recognition. *Biosens. Bioelectron.* **2017**, *94*, 148−154.
(33) Wang, P.; Xia, M.; Liang, O.; Sun, K.; Cipriano, A. F.; Schroeder, T.; Liu, H.; Xie, Y.-H. Label-Free SERS Selective

https://dx.doi.org/10.1021/acsanm.0c00846
ACS Appl. Nano Mater. 2020, 3, 5783−5793

Detection of Dopamine and Serotonin Using Graphene-Au Nanopyramid Heterostructure. *Anal. Chem.* **2015**, *87*, 10255−10261.
(34) Prochazka, M. In *Surface-Enhanced Raman Spectroscopy: Bioanalytical, Biomolecular and Medical Applications*; Springer International Publishing: Cham, 2016; pp 149−211.
(35) Prabhu, S.; Poulose, E. Silver Nanoparticles: Mechanism of Antimicrobial Action, Synthesis, Medical Applications, and Toxicity Effects. *Int. Nano Lett.* **2012**, *2*, 32.
(36) Di, H.; Liu, H.; Li, M.; Li, J.; Liu, D. High-Precision Profiling of Sialic Acid Expression in Cancer Cells and Tissues Using Background-Free Surface-Enhanced Raman Scattering Tags. *Anal. Chem.* **2017**, *89*, 5874−5881.
(37) Song, C.; Yang, B.; Yang, Y.; Wang, L. SERS-Based Mercury Ion Detections: Principles, Strategies and Recent Advances. *Sci. China: Chem.* **2016**, *59*, 16−29.
(38) Huang, G. G.; Sou, N.-L.; Hung, M.-J. Surface-Enhanced Raman Scattering Studies of The Reduction of p-Nitroaniline Catalyzed by a Nanonized Ag Porous-Glass Hybrid Composite. *Spectrochim. Acta, Part A* **2016**, *166*, 8−14.
(39) Muniz-Miranda, M. SERS Monitoring of The Catalytic Reduction of 4-Nitrophenol on Ag-Doped Titania Nanoparticles. *Appl. Catal., B* **2014**, *146*, 147−150.
(40) Syu, W.-L.; Lin, Y.-H.; Paliwal, A.; Wang, K.-S.; Liu, T.-Y. Highly Sensitive and Reproducible SERS Substrates of Bilayer Au and Ag Nano-Island Arrays by Thermal Evaporation Deposition. *Surf. Coat. Technol.* **2018**, *350*, 823−830.
(41) Oh, M.-K.; Shin, Y.-S.; Lee, C.-L.; De, R.; Kang, H.; Yu, N. E.; Kim, B. H.; Kim, J. H.; Yang, J.-K. Morphological and SERS Properties of Silver Nanorod Array Films Fabricated by Oblique Thermal Evaporation at Various Substrate Temperatures. *Nanoscale Res. Lett.* **2015**, *10*, 259.
(42) Chen, J.; Guo, L.; Qiu, B.; Lin, Z.; Wang, T. Application of Ordered Nanoparticle Self-Assemblies in Surface-Enhanced Spectroscopy. *Mater. Chem. Front.* **2018**, *2*, 835−860.
(43) Ge, M.; Li, P.; Cao, C.; Li, S.; Lin, D.; Yang, L. A Long-Period and High-Stability Three-Dimensional Surface-Enhanced Raman Scattering Hotspot Matrix. *Chem. Commun.* **2019**, *55*, 8647−8650.
(44) Zhang, K.; Ji, J.; Li, Y.; Liu, B. Interfacial Self-Assembled Functional Nanoparticle Array: A Facile Surface-Enhanced Raman Scattering Sensor for Specific Detection of Trace Analytes. *Anal. Chem.* **2014**, *86*, 6660−6665.
(45) Wu, P.; Zhong, L.-B.; Liu, Q.; Zhou, X.; Zheng, Y.-M. Polymer Induced One-Step Interfacial Self-Assembly Method for The Fabrication of Flexible, Robust and Free-Standing SERS Substrates for Rapid on-Site Detection of Pesticide Residues. *Nanoscale* **2019**, *11*, 12829−12836.
(46) Teng, Y.; Zhang, Y.; Ren, Z.; Wang, Z.; Liu, W.; Shao, K.; Pan, Z. Rapid Water/Oil Interfacial Self-Assembled Au Monolayer Nanofilm by Simple Vortex Mixing for Surface-Enhanced Raman Scattering. *New J. Chem.* **2019**, *43*, 7613−7619.
(47) Konrad, M. P.; Doherty, A. P.; Bell, S. E. J. Stable and Uniform SERS Signals from Self-Assembled Two-Dimensional Interfacial Arrays of Optically Coupled Ag Nanoparticles. *Anal. Chem.* **2013**, *85*, 6783−6789.
(48) Wu, L.; Wang, W.; Zhang, W.; Su, H.; Liu, Q.; Gu, J.; Deng, T.; Zhang, D. Highly Sensitive, Reproducible and Uniform SERS Substrates with a High Density of Three-Dimensionally Distributed Hotspots: Gyroid-Structured Au Periodic Metallic Materials. *NPG Asia Mater.* **2018**, *10*, No. e462.
(49) Hwang, J. S.; Yang, M. Sensitive and Reproducible Gold SERS Sensor Based on Interference Lithography and Electrophoretic Deposition. *Sensors* **2018**, *18*, 4076.
(50) Xu, D.; Teng, F.; Wang, Z.; Lu, N. Droplet-Confined Electroless Deposition of Silver Nanoparticles on Ordered Superhydrophobic Structures for High Uniform SERS Measurements. *ACS Appl. Mater. Interfaces* **2017**, *9*, 21548−21553.
(51) Jiang, S.; Guo, J.; Zhang, C.; Li, C.; Wang, M.; Li, Z.; Gao, S.; Chen, P.; Si, H.; Xu, S. A sensitive, Uniform, Reproducible and Stable SERS Substrate Has been Presented Based on MoS_2@Ag Nanoparticles@Pyramidal Silicon. *RSC Adv.* **2017**, *7*, 5764−5773.
(52) Schmidt, M. S.; Boisen, A.; Hübner, J. In *Towards Easily Reproducible Nano-Structured SERS Substrates, SENSORS*; IEEE: Christchurch, 2009; pp 1763−1767.
(53) Wang, T.; Zhou, J.; Wang, Y. Simple, Low-Cost Fabrication of Highly Uniform and Reproducible SERS Substrates Composed of Ag−Pt Nanoparticles. *Nanomaterials* **2018**, *8*, 331.
(54) Ren, W.; Fang, Y.; Wang, E. A Binary Functional Substrate for Enrichment and Ultrasensitive SERS Spectroscopic Detection of Folic Acid Using Graphene Oxide/Ag Nanoparticle Hybrids. *ACS Nano* **2011**, *5*, 6425−6433.
(55) Nie, R.; Wang, J.; Wang, L.; Qin, Y.; Chen, P.; Hou, Z. Platinum Supported on Reduced Graphene Oxide as a Catalyst for Hydrogenation of Nitroarenes. *Carbon* **2012**, *50*, 586−596.
(56) Liu, Y.; Hu, Y.; Zhang, J. Few-Layer Graphene-Encapsulated Metal Nanoparticles for Surface-Enhanced Raman Spectroscopy. *J. Phys. Chem. C* **2014**, *118*, 8993−8998.
(57) Neri, G.; Fazio, E.; Mineo, P. G.; Scala, A.; Piperno, A. SERS Sensing Properties of New Graphene/Gold Nanocomposite. *Nanomaterials* **2019**, *9*, 1236.
(58) Tatarkin, D. E.; Yakubovsky, D. I.; Ermolaev, G. A.; Stebunov, Y. V.; Voronov, A. A.; Arsenin, A. V.; Volkov, V. S.; Novikov, S. M. Surface-Enhanced Raman Spectroscopy on Hybrid Graphene/Gold Substrates Near the Percolation Threshold. *Nanomaterials* **2020**, *10*, 164.
(59) Liu, Y.; Luo, F. Large-Scale Highly Ordered Periodic Au Nano-Discs/Graphene and Graphene/Au Nanoholes Plasmonic Substrates for Surface-Enhanced Raman Scattering. *Nano Res.* **2019**, *12*, 2788−2795.
(60) Nair, A. K.; Bhavitha, K. B.; Perumbilavil, S.; Sankar, P.; Rouxel, D.; Kala, M. S.; Thomas, S.; Kalarikkal, N. Multifunctional Nitrogen Sulfur Co-Doped Reduced Graphene Oxide − Ag Nano Hybrids (Sphere, Cube and Wire) for Nonlinear Optical and SERS Applications. *Carbon* **2018**, *132*, 380−393.
(61) He, S.; Liu, K.-K.; Su, S.; Yan, J.; Mao, X.; Wang, D.; He, Y.; Li, L.-J.; Song, S.; Fan, C. Graphene-Based High-Efficiency Surface-Enhanced Raman Scattering-Active Platform for Sensitive and Multiplex DNA Detection. *Anal. Chem.* **2012**, *84*, 4622−4627.
(62) Ma, D.; Li, S.; Liang, C. Electropolishing of High-Purity Aluminium in Perchloric Acid and Ethanol Solutions. *Corros. Sci.* **2009**, *51*, 713−718.
(63) Kuo, C.-C.; Chen, C.-H. Graphene Thickness-Controlled Photocatalysis and Surface Enhanced Raman Scattering. *Nanoscale* **2014**, *6*, 12805−12813.
(64) Neufeld, P.; Southall, D. M. The Electropolishing of Aluminum. *Electrodeposition Surf. Treat.* **1975**, *3*, 159−168.
(65) Lee, S.; Lee, K.; Zhong, Z. Wafer Scale Homogeneous Bilayer Graphene Films by Chemical Vapor Deposition. *Nano Lett.* **2010**, *10*, 4702−4707.
(66) Ferrari, A. C.; Meyer, J. C.; Scardaci, V.; Casiraghi, C.; Lazzeri, M.; Mauri, F.; Piscanec, S.; Jiang, D.; Novoselov, K. S.; Roth, S.; Geim, A. K. Raman Spectrum of Graphene and Graphene Layers. *Phys. Rev. Lett.* **2006**, *97*, 187401.
(67) Kim, K.; Lee, H. B.; Shin, D.; Ryoo, H.; Lee, J. W.; Shin, K. S. Surface-Enhanced Raman Scattering of 4-Aminobenzenethiol on Silver: Confirmation of the Origin of b_2-Type Bands. *J. Raman Spectrosc.* **2011**, *42*, 2112−2118.
(68) Shin, K. S. Effect of Surface Morphology on Surface-Enhanced Raman Scattering of 4-Aminobenzenethiol Adsorbed on Gold substrates. *J. Raman Spectrosc.* **2008**, *39*, 468−473.
(69) Kim, K.; Yoon, J. K. Raman Scattering of 4-Aminobenzenethiol Sandwiched between Ag/Au Nanoparticle and Macroscopically Smooth Au Substrate. *J. Phys. Chem. B* **2005**, *109*, 20731−20736.
(70) Park, W.-H.; Kim, Z. H. Charge Transfer Enhancement in the SERS of a Single Molecule. *Nano Lett.* **2010**, *10*, 4040−4048.
(71) Takeyasu, N.; Kagawa, R.; Sakata, K.; Kaneta, T. Laser Power Threshold of Chemical Transformation on Highly Uniform

https://dx.doi.org/10.1021/acsanm.0c00846
ACS Appl. Nano Mater. 2020, 3, 5783−5793

Plasmonic and Catalytic Nanosurface. *J. Phys. Chem. C* **2016**, *120*, 12163−12169.
(72) Huang, Y.-F.; Zhu, H.-P.; Liu, G.-K.; Wu, D.-Y.; Ren, B.; Tian, Z.-Q. When the Signal Is Not from the Original Molecule To Be Detected: Chemical Transformation of para-Aminothiophenol on Ag during the SERS Measurement. *J. Am. Chem. Soc.* **2010**, *132*, 9244−9246.
(73) Pokrovski, G.; Akinfiev, N.; Borisova, A.; Zotov, A.; Kouzmanov, K. In *Gold-Transporting Hydrothermal Fluids in the Earth's Crust*; Geological Society of London, 2014; pp 9−70.
(74) Li, L.-M.; Fang, P.-P.; Yang, Z.; Huang, W.-D.; Wu, D.; Ren, B.; Tian, Z.-Q. Size Dependent SERS Activity of Gold Nanoparticles Studied by 3D-FDTD Simulation. *Spectrosc. Spect. Anal.* **2009**, *29*, 1222−1226.
(75) Wei, A.; Kim, B.; Sadtler, B.; Tripp, S. L. Tunable Surface-Enhanced Raman Scattering from Large Gold Nanoparticle Arrays. *ChemPhysChem* **2001**, *2*, 743−745.
(76) Liu, K.-K.; Tadepalli, S.; Tian, L.; Singamaneni, S. Size-Dependent Surface Enhanced Raman Scattering Activity of Plasmonic Nanorattles. *Chem. Mater.* **2015**, *27*, 5261−5270.

https://dx.doi.org/10.1021/acsanm.0c00846
ACS Appl. Nano Mater. 2020, 3, 5783−5793